

Discovery of *N*-[(2*S*)-5-(6-Fluoro-3-pyridinyl)-2,3-dihydro-1*H*-inden-2-yl]-2-propanesulfonamide, a Novel Clinical AMPA Receptor Positive Modulator[†]

Simon E. Ward,^{*,‡} Mark Harries,[‡] Laura Aldegheri,[§] Daniele Andreotti,[§] Stuart Ballantine,^{||} Benjamin D. Bax,^{||} Andrew J. Harris,[‡] Andy J. Harker,[‡] Jesper Lund,[§] Rosemary Melarange,[‡] Anna Mingardi,[§] Claudette Mookherjee,[‡] Julie Mosley,^{||} Marta Neve,[§] Beatrice Oliosi,[§] Roberto Profeta,[§] Kathrine J. Smith,^{||} Paul W. Smith,[‡] Simone Spada,[§] Kevin M. Thewlis,[‡] and Shahnaz P. Yusuf^{||}

[‡]Neurosciences Centre of Excellence for Drug Discovery, GlaxoSmithKline, New Frontiers Science Park, Third Avenue, Harlow, Essex CM19 5AW, United Kingdom, [§]Centro Ricerche, GlaxoSmithKline, Via A. Fleming 4, 37100 Verona, Italy, and

^{||}Molecular Discovery Research, GlaxoSmithKline, Medicines Research Centre, Gunnels Wood Road, Stevenage SG1 2NY, United Kingdom

Received May 5, 2010

A series of AMPA receptor positive allosteric modulators has been optimized from poorly penetrant leads to identify molecules with excellent preclinical pharmacokinetics and CNS penetration. These discoveries led to **17i**, a potent, efficacious CNS penetrant molecule with an excellent pharmacokinetic profile across preclinical species, which is well tolerated and is also orally bioavailable in humans.

Introduction

A growing body of evidence indicates that dysfunction of glutamatergic neurotransmission underlies the pathophysiology of many neurological diseases including schizophrenia, Alzheimer's disease, Parkinson's disease, and mood disorders.^{1,2} Preclinical studies have identified modulators of the α -amino-3-hydroxyl-5-methyl-4-isoxazole-propionic acid receptor (AMPA-R^c), which slow the rate of receptor deactivation and/or desensitization, leading to enhanced synaptic activity and efficacy in cognition models.^{3–5}

AMPA belong to the ligand-gated, ionotropic glutamatergic receptor family and are widely distributed in the mammalian central nervous system and mediate the vast majority of fast excitatory neurotransmission in the CNS.^{6,7} The receptors are tetrameric assemblies of subunits GluA1–4 (originally named GluR1–4 or GluRA–D), in which two subunits join to form a dimer which then combine to form a tetrameric complex.^{8,9} Each subunit comprises a large extracellular domain incorporating the glutamate binding residues in the ligand-binding domain (LBD),¹⁰ three hydrophilic regions (M1, M3 and M4) which span the membrane and a re-entrant

loop (M2) which constitutes part of the ion channel pore,¹¹ and an intracellular domain comprising motifs for binding and phosphorylation of transmembrane AMPA regulatory proteins (TARPs) which play a pivotal role in regulating the trafficking of AMPARs during synaptic plasticity.¹² These AMPAR auxiliary subunits are also fundamental to synaptic transmission within the CNS modulating open channel probability and channel kinetics,¹³ single channel conductance,¹⁴ and sensitivity to polyamine block.¹⁵

The understanding of the biophysical and structural characteristics of the AMPAR has advanced considerably over the past decade, in particular through investigation of the AMPAR ligand-binding core, which is formed by two polypeptide segments S1, located at the M1 region, and S2, located between M3 and M4 regions. Studies have shown that the S1S2 domain possesses pharmacological properties that are similar to those of native membrane bound receptors.¹⁶ The crystal structure of the rat GluA2 S1S2 ligand binding domain has allowed development of agonists and antagonists which have benefited from high resolution structural information.¹⁷ More recent studies have identified binding sites for positive allosteric modulators of AMPAR and investigated mechanisms by which such molecules exert their pharmacological effects acting to slow both agonist release and rate of receptor deactivation.¹⁸ Most recently, this structural investigation has been taken to even greater ends with the successful crystallization and structural elucidation of the rat GluA2 receptor at 3.6 Å in complex with a competitive antagonist.¹⁹

Despite these advances in basic understanding, designing molecules to potentiate ion flux through the AMPAR remains challenging, not least due to the layers of complexity created by the existence of a number of splice variants²⁰ and sites for post-translational modification which influence receptor kinetics²¹ and binding.²² All in all, this serves to render the specific composition of ion channels in vivo extremely complicated and one of the key challenges faced by a drug discovery program is to have confidence that data generated

[†]The atomic coordinates for the crystal structure of **17i** described here have been deposited at the Protein Data Bank under entry code 2xhd.

*To whom correspondence should be addressed. Phone: +44 (0) 1279 622894. Fax: +44 1279 622 790. E-mail: simon.e.ward@gsk.com.

^a Abbreviations: AMPA, α -amino-3-hydroxyl-5-methyl-4-isoxazole-propionate; AMPAR, AMPA receptor; AUC, area under the curve; BTB, brain tissue binding; CNS, central nervous system; DBU, 1,8-diazabicyclo[5.4.0]undec-7-ene; DTT, dithiothreitol; IV, intravenous; FLIPR, fluorescent imaging plate reader; GPCR, G-protein coupled receptor; hERG, human ether-a-go-go related gene; IPTG, isopropyl- β -D-thiogalactopyranoside; LBD, ligand-binding domain; LTP, long-term potentiation; MDCK, Madin–Darby canine; MDR, multidrug-resistant; NADPH, nicotinamide adenosine dinucleotide phosphate; NMDA, *N*-methyl-D-aspartic acid; NOAEL, no observed adverse event level; NOR, novel object recognition; P-gp, P-glycoprotein; PPB, plasma protein binding; PSA, polar surface area; PXR, pregnane X receptor; SD, standard deviation; TARP, transmembrane AMPA regulatory protein.

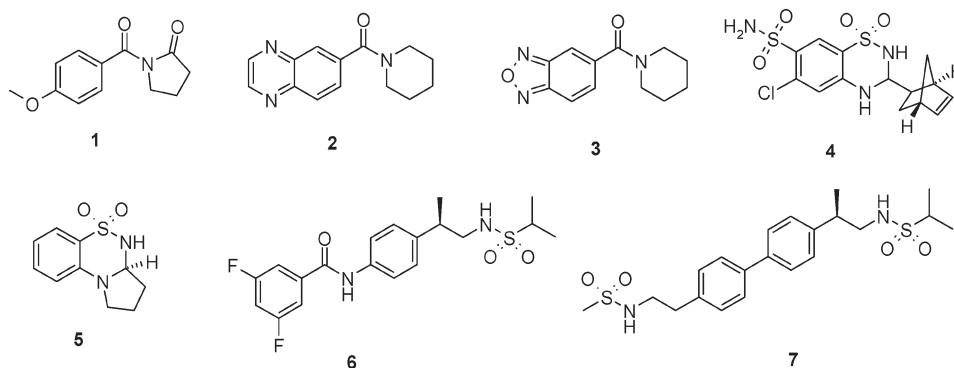
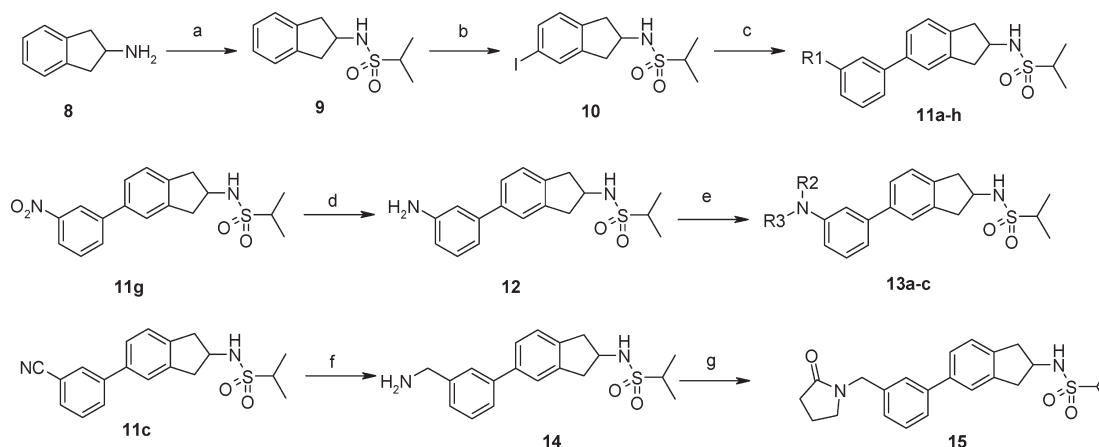


Figure 1. Clinically evaluated AMPAR positive modulators.

Scheme 1. Synthesis of Phenyl Indane Analogues^a



^a Reagent and reaction conditions: (a) DBU, CH_2Cl_2 , ${}^i\text{PrSO}_2\text{Cl}$; (b) periodic acid, I_2 , AcOH , H_2SO_4 ; (c) 3- R^1 -phenyl boronic acid, Cs_2CO_3 , $\text{Pd}(\text{OAc})_2$, PPh_3 , dioxane; (d) 10% Pd/C , EtOH , H_2 ; (e) for **13a** ${}^i\text{PrCOCl}$, for **13b** EtSO_2Cl , for **13c** 3-chloropropanesulfonyl chloride Et_3N , DMF ; (f) LiAlH_4 , THF , 0°C ; (g) 4-chlorobutanoyl chloride, Et_3N , CH_2Cl_2 .

against recombinant systems will translate reliably through to the native system.

Many molecules have been described as AMPAR positive modulators across a range of chemotypes^{23,24} which, despite differences in their proposed mechanism, promote long-term potentiation (LTP)^{23,24} by enhancing glutamatergic synaptic activity. LTP is thought to be the underlying mechanism for cognition^{23,24} and as such, preclinical cognition models have been the primary focus for AMPAR modulators although the aim is to progress molecules in the clinic to treat a range of diseases such as schizophrenia, depression, and Parkinson's disease.^{23,24} In brief, three major, well-established classes that have been investigated clinically exist alongside a number of less extensively exemplified structures (Figure 1). The first main group derives from the original nootropic agent **1** (Aniracetam) and were subsequently developed into a range of benzamide derivatives by Cortex including **2** (CX-516) and **3** (CX-691). The second major class, benzothiadiazines, exemplified by the diuretic agent **4** (cyclothiazide) was developed into **5** (S-18986) by Servier. The third broad class comprises the phenethylsulfonamides discovered by Lilly, which include clinically investigated **6** (LY450108) and **7** (LY451395). In broad terms the molecules have generally displayed higher affinities for the AMPAR over time, with the Lilly phenethylsulfonamides being considerably more potent than the original benzamide class.

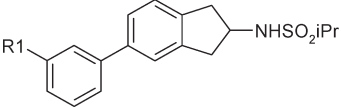
From evaluation of these chemotypes, we sought to initiate a program to create our own series of CNS-penetrant

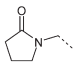
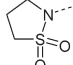
AMPA positive modulators, in particular combining high potency with a pharmacokinetic profile which would deliver high, unbound compound concentrations.²⁵

Results

Preparation of Phenyl Indane Analogues. Our initial exploratory activities identified **11a** as the lead for this program. The indane analogues were prepared from amino indane **8** as described in Scheme 1 via sequential functionalization to first form the sulfonamide **9** and then the regioselective iodinated derivative **10**. This reaction was unsuccessful on the parent amino indane due to a lack of regiochemical control. Key intermediate **10** was then reacted under standard Suzuki coupling conditions to afford a range of analogues **11a–h**. Certain of these were reacted further to broaden the scope of the chemotypes investigated. In particular, nitro derivative **11g** was hydrogenated to afford aniline derivative **12**, which could be acylated or sulfonylated to afford a wider range of amides and sulfonamides **13a–c**. Nitrile derivative **11c** was also used as the starting point for analogues, with a methylene spacer between the phenyl ring and nitrogen atom by subjecting **11c** to sequential reduction with lithium aluminum hydride to amine **14** and acylation to lactam **15**.

Pharmacological Characterization of Analogues. The ability of the test compounds to potentiate a glutamate receptor-mediated response was determined primarily by using fluorescent calcium-indicator dyes and then additionally for some

Table 1. Biological Activity and Physicochemical Data for 3-Substituted Phenyl Indane Analogues^a


Cpd	R1	pEC ₅₀	Asym Max	PSA (Å ²)	MWt	clogP ^b	%rat PPB ^c
6		6.4	121%	75	396.5	3.5	
11a	NHSO ₂ Me	6.1	123%	92	409	2.7	95.9
11b	SO ₂ NMe ₂	5.1	30%	84	423	3.0	-
11c	CN	<4.3	48%	70	340	3.3	-
11d	COMe	<4.3	31%	63	357	3.3	-
11e	CH ₂ COMe	5.2	75%	63	372	3.1	-
11f	NHCOMe	4.7	54%	75	360	3.6	94.9
13a	NHCO ^t Pr	<4.3	-	75	401	3.7	-
15		4.9	40%	66	413	2.7	97.6
13b	NHSO ₂ Et	5.6	101%	92	423	3.2	-
11h	NMeSO ₂ Me	5.9	105%	84	423	2.7	96.4
13c		6.4	118%	84	434	2.8	96.7

^a FLIPR generated pEC₅₀ against hGluA2 flip isoform. All values are ±0.2 and $n = 3$ except for **11h** ($n = 2$). Asym max is the fitted maximum response, relative to 100% defined as the maximal response of cyclothiazide standard. ^b clogP Daylight Chemical Information Systems Inc., Aliso Viejo, CA, <http://www.daylight.com>. ^c Rat plasma protein binding (rat PPB) values were determined using a 96-well plate equilibrium dialysis method at a concentration of 1 μg/mL.

example compounds by measuring glutamate-evoked currents recorded from human GluA2 flip (hGluA2i), Q/R unedited HEK293 cells. For the primary screen against hGluA2i homomeric AMPARs, a concentration–response curve was derived for potentiation of glutamate-induced rises in intracellular calcium. Further data also confirmed, for those molecules profiled, a broad spectrum positive modulatory activity across AMPARs formed from different subunits (GluA1i, GluA3i, or GluA4i homomers) and also equivalent potency at rat and human GluA2i homomeric AMPARs.

As detailed in Table 1, lead **11a** displayed potent potentiation of the AMPAR-mediated response, with encouraging predicted physicochemical properties: low clogP and moderate molecular weight, contributing to acceptable rat plasma protein binding of 95.9%. Furthermore, this molecule had a clean selectivity profile against key targets and did not inhibit P450 enzymes at low concentrations (data not shown). **11a** was also progressed to a rat oral pharmacokinetic study and, very encouragingly, gave excellent systemic exposure and time-course profile. However, as detailed in Table 2 and most likely as a consequence of the high polar surface area, this molecule suffered restricted access to the brain due to interaction with P-glycoprotein (P-gp).²⁶ This was supported by experimental data showing a moderate to high efflux ratio in the MDCK-MDR1 in vitro P-gp assay.

It was clear from our preliminary investigation that modification of the secondary sulfonamide group attached to the indane was not tolerated; the presence of both the secondary nitrogen and sulfonyl group were crucial for activity. As such, analogue investigation focused on the substituent on the phenyl ring, which was restricted to the *meta* position, as

Table 2. Rat Pharmacokinetic (PK) Profiles of Key 3-Phenyl Substituted Indanes

compd	AUC _{0–t} ng·h/mL	Brain:Blood AUC _{0–t} ratio	PAPP(+inh) nm/s ^a	efflux ratio
11a	1130	0.1	608	5.8
11h	161	0.4	698	3.2
15	36	0.4		

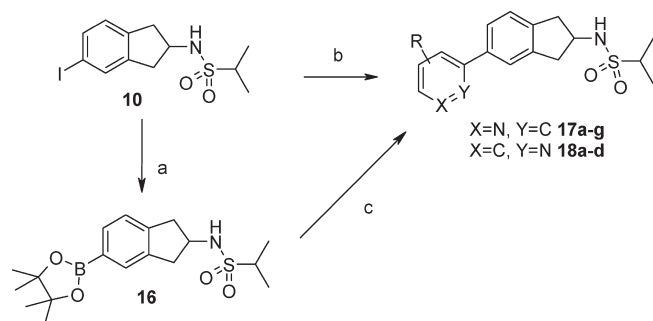
^a PAPP (+inh): apical (A) to basolateral (B) transport rates of molecules (0.5 μM) across Madin–Darby canine multidrug-resistant (MDCKII-MDR1) cells heterogeneously expressing human P-gp measured in presence of a potent P-gp inhibitor, GF120918, as an indicator of passive membrane permeability. Efflux ratio: the ratio of transport from A–B/B–A in the absence of P-gp inhibitor (inh).

their regioisomeric analogues demonstrated lower potencies. Removal of this substituent led to a loss of activity, which could not be restored by installing other polar, hydrogen-bond accepting groups such as reversed sulfonamide **11b**, nitrile **11c**, or ketone **11d**. Recognizing that the hydrogen bond acceptor may need to be separated from the phenyl group by a spacer atom, we prepared the homologated ketone **11e** and the methylene-linked lactam **15**, both of which were only moderately active compounds. Similarly, replacement of the sulfonamide group in **11a** with an amide **11f** led to a loss of activity, which was exacerbated by increasing the size of the alkyl group to isopropyl **13a**. The only substituents which maintained good potency were the sulfonamides, for which larger alkyls **13b** and tertiary sulfonamides **11h** and **13c** gave high potency, demonstrating the tolerance for increased size and loss of the H-bond donor capability. Furthermore, this meant that all highly active compounds, regardless of clogP, had a high polar surface area, although only ethyl sulfonamide **13b** was as high as lead **11a**.

With this in mind, we profiled further exemplars from this set in rat pharmacokinetic studies. Unfortunately, as outlined in Table 2, although brain–blood AUC ratios for the tertiary amide **15** and the tertiary sulfonamide analogue **11h** were improved, and acceptable protein binding maintained, systemic exposures were poor.

Preparation and Characterization of Pyridyl Indane Analogues. Given the challenges we had encountered in balancing potency with CNS penetration, and despite the lack of success in truncating the sulfonamide substituent in lead **11a**, we decided to explore the indane substituent with a range of alternative aromatic rings which would all be of significantly lower polar surface area. By doing so, we hoped to decrease interaction with P-gp, while maintaining good systemic free concentrations thereby maximizing the free drug

Scheme 2. Preparation of Pyridyl Indane Analogues^a



^a Reagent and reaction conditions: (a) (1,1'-bis(diphenylphosphino)ferrocene)palladium(II) chloride, CH₂Cl₂, KOAc, bis(pinacolato)diboron, DMSO; (b) Cs₂CO₃, R-substituted bromopyridine, Pd(OAc)₂, PPh₃, dioxane; (c) Cs₂CO₃, R-substituted pyridyl boronic acid, Pd(OAc)₂, PPh₃, dioxane.

concentrations in the brain, even if potentially at the expense of high potency. A number of systems were investigated, and by far the most effective were the pyridines, in particular, the 3-pyridyl and 2-pyridyl indane analogues. The initial compound sets were prepared as described in Scheme 2. Use of earlier key intermediate **10** allowed for rapid preparation of these derivatives, with the route chosen according to the availability of the pyridyl boronic acid coupling partners. Intermediate **10** was therefore either reacted directly under Suzuki cross-coupling conditions with substituted pyridyl boronic acids to afford the final pyridyl derivatives **17a–g** and **18a–d**, or via a two-step process first involving preparation of the indane boronate ester species **16** with subsequent cross-coupling to afford the target molecules. While these are short synthetic sequences, the precise conditions of the Suzuki coupling required considerably more optimization and were generally lower yielding than for phenyl analogues above.

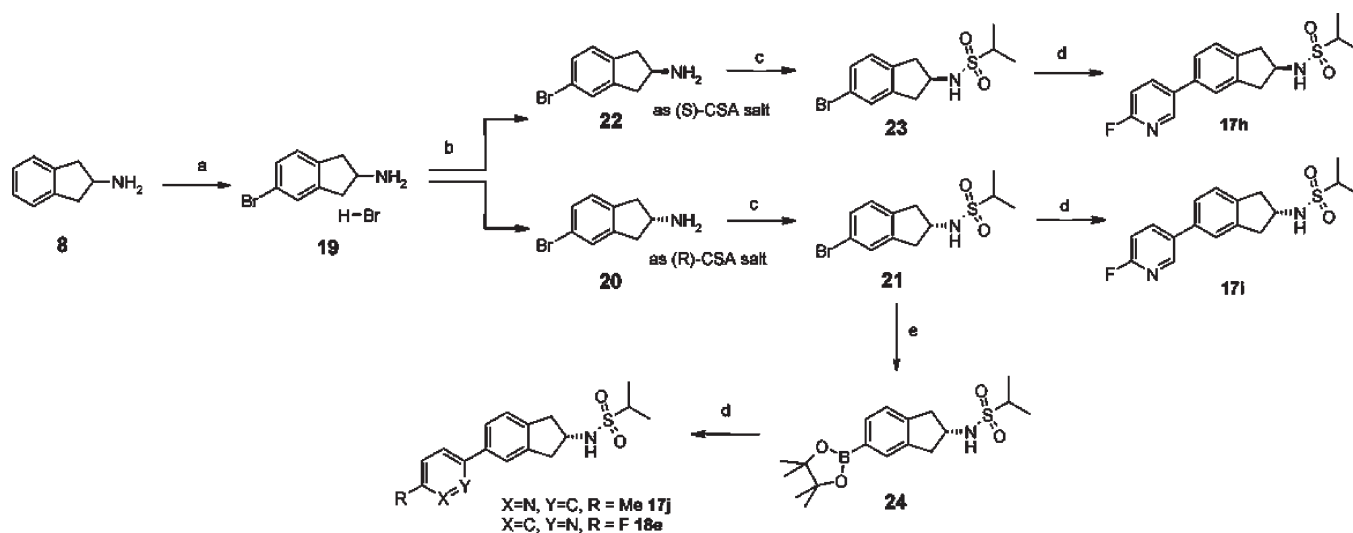
As displayed in Table 3, the initial analogue in this set, unsubstituted 3-pyridyl indane **17a**, gave lower activity in the primary screen, in line with previously established SAR, coupled with inhibition of P450 1A2 isoform and moderate intrinsic clearance in rat microsomes. However, this analogue had significantly improved physicochemical properties: lower polar surface area, molecular weight, and calculated lipophilicity. As such, we wanted to further investigate the potential of these pyridyl derivatives, but in order to maintain a low polar surface area to maximize our chances of improving CNS penetration, we were severely restricted in the range of substituents available for use. This is highlighted by inclusion of the cyano pyridyl derivative **17e** in the data set, for which the PSA is restored to an unacceptably high value of 83 Å².

Consequently, the range of substituents explored centered on alkyl and halo derivatives, which gave a range of properties

Table 3. Biological and in Vitro DMPK Profiling of Novel Pyridyl Indane Analogues^a

compd	R	<i>f</i>	pEC ₅₀	Asym max %	PSA (Å ²)	MWt	clogP ^g	pK _a ^b	P450 (μM) ^c					CLi ^d (mL/min/g)	
									1A2	2C9	2C19	2D6	3A4	rat	human
3-Pyridyls															
17a	H	rac	4.8	101	59	316	2.3	5.1	0.6	>10	>10	>10	>10	2.1	<0.5
17b	2-F	rac	4.8	96	59	334	2.6	<i>e</i>	>10	>10	9.0	>10	>10	2.5	2.1
17c	6-F	rac	5.3	106	59	334	2.6	<i>e</i>	>10	>10	>10	>10	>10	1.1	1.7
17d	2,6-diMe	rac	4.5	59	59	344	3.0	6.7	>10	>10	>10	>10	>10	4.9	0.9
17e	5-CN	rac	4.2	84	83	341	2.0	<i>e</i>	>10	>10	>10	>10	>10	<0.5	0.7
17f	4-Me	rac	4.7	64	59	330	2.5	5.8	>10	>10	>10	>10	>9	4.5	1.4
17g	6-Me	rac	5.5	107	59	330	2.8	5.7	>10	>10	>10	>10	>10	2.0	0.7
17h	6-F	<i>R</i>	<4.5		59	334	2.6	<i>e</i>							
17i	6-F	<i>S</i>	5.6	107	59	334	2.6	<i>e</i>	>10	>10	>10	>10	>10	0.7	<0.7
17j	6-Me	<i>S</i>	5.7	104	59	330	2.8	5.8	>10	>10	>10	>10	>10	3.5	<0.6
2-Pyridyls															
18a	5-F	rac	5.2	114	59	334	2.8	2.7	>10	>10	>10	>10	>10	0.6	0.5
18b	5-Me	rac	5.5	90	59	330	3.0	4.9	>10	>10	>10	>10	>10	7.3	0.8
18c	3-Me	rac	4.7	89	59	330	2.8	4.9	>10	>10	>10	>10	>10	14	1.3
18d	5-Cl	rac	5.1	89	59	351	3.4		>10	>10	>10	>10	>10	<0.8	<0.5
18e	5-F	<i>S</i>	5.7	103	59	334	2.8	2.7	>10	>10	>10	>10	>10	1.6	<0.5

^a FLIPR generated pEC₅₀ against hGluA2 flip isoform. All values are ±0.2 and *n* ≥ 3. Asym max is the fitted maximum response, relative to 100% defined as the maximal response of cyclothiazide standard. ^b pK_a measured spectroscopically. ^c Inhibition of P450 isoforms. ^d Rate of turnover against rat and human liver microsomes. ^e No pK_a could be determined. ^f stereochemistry at chiral center, rac = racemic mixture. ^g clogP Daylight Chemical Information Systems Inc., Aliso Viejo, CA, <http://www.daylight.com>.

Scheme 3. Preparation of Single Enantiomer Pyridyl Indane Analogues^a

^a Reagent and reaction conditions: (a) (i) HCl, water, (ii) Br₂, (iii) HBr; (b) 4-methylmorpholine (*R*)-CSA or (*S*)-CSA, MeOH; (c) (i) 1 M NaOH, CH₂Cl₂, (ii) ^tPrSO₂Cl, DBU, CH₂Cl₂; (d) pyridyl boronic acid or substituted bromo-pyridine, Pd(Ph₃)₄, H₂O/1,4-dioxan, Cs₂CO₃; (e) Bis(pinacolato) diboron, KOAc, PdCl₂(dppf), DMSO.

in terms of pyridine conjugate acid p*K*_a, EC₅₀, and stability to microsomal turnover. For the 3-pyridyl indanes, a substituent *para* to the indane group on the pyridine ring gave an increase in potency as exemplified by the fluorine in **17c** and the methyl in **17g**. The P450 inhibition profile across the set **17b–g** appeared to show an improvement over initial unsubstituted derivative **17a**, even for analogue **17f**, with no substituent on the carbon adjacent to the pyridine nitrogen. The intrinsic clearance for this set was more variable: fluorine on the carbon adjacent to the pyridine nitrogen increased microsomal turnover in human. The methyl substituted pyridines **17d**, **17f**, and **17g** showed higher microsomal turnover in rat. As expected, all methyl substituted pyridines are significantly more basic than their halogenated counterparts, for which no p*K*_a of the conjugate acid could be determined. However, we were unable to determine whether the increased rat microsomal turnover was due solely to the increased basicity of the pyridine or instead was simply a consequence of the methyl group being a site of potential metabolism.

A similar pattern was replicated for the 2-pyridyl indane analogues **18a–d**. The best AMPAR potentiation potencies were observed for substituents *para* to the indane ring for fluoro derivative **18a** and methyl derivative **18b**, and all compounds demonstrated an excellent profile against the P450 isoform panel. Similarly to the previous group, more basic pyridines **18b** and **18c** were turned over to a far greater extent by rat microsomes than halo analogues **18a** and **18d**.

Before committing to further activities in this area, we ran a series of screening CNS penetration studies in the rat, which validated our hypothesis of lowering PSA to drive improved PK profiles. Key exemplars **17b** and **17g** were dosed to rat and found to have brain–blood ratios of 1.5:1 and 1.4:1 respectively. This data set gave us the confidence to continue exploration in this area and required us to optimize our synthetic sequences to allow exploration in the single enantiomer series.

Preparation and Characterization of Single Enantiomeric Indanes. Because of the difficulties in separating the individual enantiomers of the molecules above and the desire to prepare sufficient quantities of compound for *in vivo* biological testing,

we sought to identify an improved synthetic route. Scheme 3 outlines the revised synthetic procedure, which drew on a published classical resolution as the most pragmatic and efficient way to access single enantiomer materials.²⁷ Direct bromination of amino indane **8** generated the hydrobromide salt of 5-bromoindane derivative **19** in excellent yield. This material could then be efficiently resolved into its constituent enantiomers **20** and **22** using the required enantiomer of camphor sulfonic acid. The seemingly straightforward sulfonylation required considerable optimization to allow isolation of **21** or **23** in high yield, which was then reacted, as before, under Suzuki cross-coupling conditions to give target compounds **17i** or an enantiomeric analogue such as **17h**. Transformation of intermediate **21** into the corresponding boronic ester **24** allowed preparation of target compounds **17j** and **18e** after the Suzuki cross coupling.

As shown in Table 3, racemic **17c** comprised *R* enantiomer **17h** and *S* enantiomer **17i**, the latter being considerably more potent, and as such, exploration in the single enantiomer series focused exclusively on the *S* stereochemistry series. The three enantiomers characterized in detail, **17i**, **17j**, and **18e**, showed good potentiation of AMPA currents, a lack of P450 isoform inhibition, and intrinsic clearance in line with the racemic analogues: low turnover for fluoro analogues **17i** and **18e** in rat and human microsomes with moderate turnover in the rat system for methyl pyridine **17j**. All three of these compounds showed excellent wider selectivity against a wide range of other ion channels (including hERG, NMDA, and kainate channels), enzymes, and GPCRs. Furthermore, as shown in Figure 2, analogues showed clear potentiation of AMPAR-mediated currents in whole-cell patch-clamp electrophysiology evaluation of the recombinant hGluA2i cell line.

Molecules **17i** and **18e** were also investigated in behavioral models of cognition and found to improve performance in rats. Specifically, **17i** and **18e** (administered by oral gavage as suspension in methyl cellulose solution) were tested for their ability to improve a 24 h delay-induced deficit in novel object recognition (NOR),²⁸ a test of recognition memory in male Lister Hooded rats (*n* = 9–12/group). Following single oral

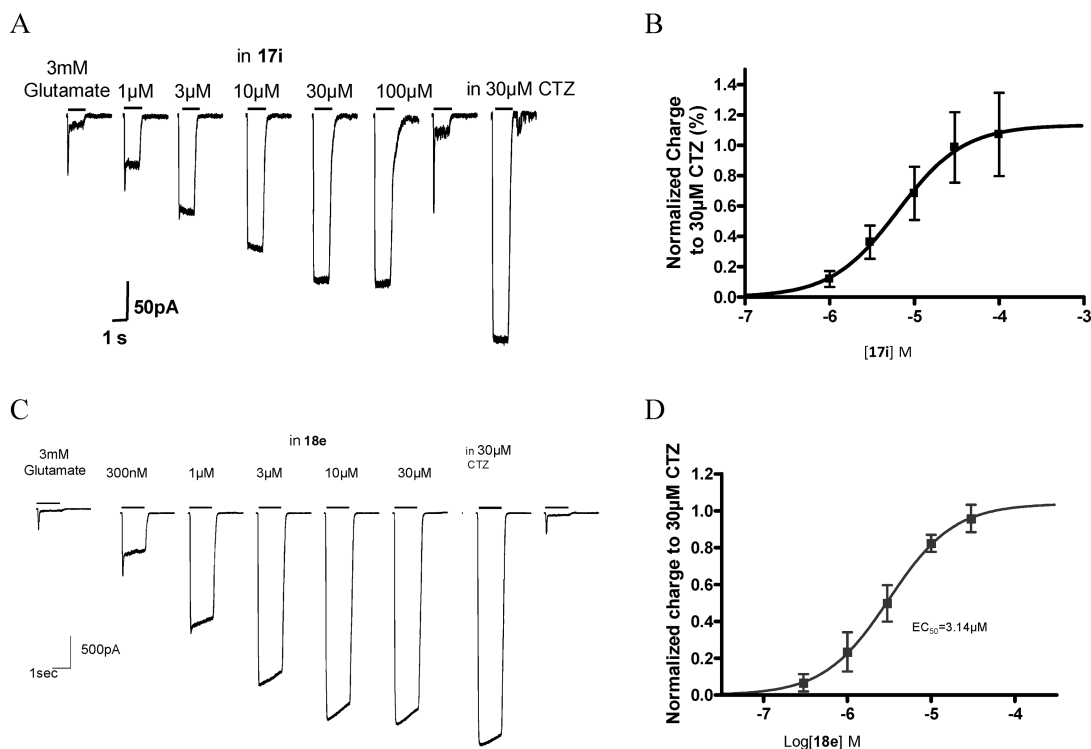


Figure 2. Electrophysiological activity of lead analogues. (A) Representative whole-cell current traces recorded from HEK293 cell expressing hGluA2i homomeric AMPARs. **17i** (1–100 μM, upper concentration limited by solubility) produced a concentration-dependent and reversible increase in charge transfer. Positive modulator, cyclothiazide (CTZ) 30 μM, also increased charge transfer. (B) Concentration–response curve for the potentiation of hGluA2i-mediated inward currents by **17i**. Each data point is the mean response from four different cells and is normalized to the effect of 30 μM cyclothiazide. $pEC_{50} = 5.19$. (C,D) Same data plots for **18e**.

administration, both molecules improved performance in this task with a minimally effective dose (MED) of 0.3 mg/kg (equivalent to concentrations of 81 ng/mL blood and 122 ng/g brain for **17i**, and 37 ng/mL blood and 70 ng/g brain for **18e**). In the passive avoidance task,²⁹ scopolamine administration (0.8 mg/kg, intraperitoneal) at 6 h post-training rendered experimentally naïve male Wistar rats ($n = 6–12$ /group) amnesic when tested 24 h later. **17i** and **18e** (administered as for NOR) 3 h prior to training dose-dependently attenuated the scopolamine-induced amnesic deficit with significant effects at 3 and 10 mg/kg for **17i** and 1 and 3 mg/kg for **18e** (no concentration data available). The compounds administered in the absence of scopolamine had no effect on recall of the passive avoidance response nor any effect on locomotor activity as assessed in an open-field arena.

Comparison of the DMPK properties for **17i**, **17j**, and **18e**, detailed in Table 4, confirms all three molecules had good permeability, were not P-gp substrates, showed good CNS penetration together with good free fraction, and satisfactory rat pharmacokinetics. Blood clearance was low for **17i** and low to moderate for **18e**. The rank order of in vivo clearance for the three molecules in rat was consistent with that found in vitro, with **17j** showing the greatest clearance. Volume of distribution was moderate and appeared to be similar for all 3 molecules; however as a result of the moderate/high clearance, **17j** gave the shortest half-life (< 1 h) and the lowest oral bioavailability. In addition, in vitro microsomal clearance across species appeared to be higher for **17j**, suggesting lower oral exposure across species and potentially in humans.

From the efficacy and DMPK data, both **17i** and **18e** were progressed to safety and tolerability studies and **17i** was selected as the molecule to advance as a clinical drug candidate.

Detailed Evaluation of Preclinical Profile of 17i. In contrast to the more basic pyridine analogues, the equilibrium solubility of **17i** was uniformly low (0.1 mg/mL or less) across the pH range 2–10 and in the physiologically relevant fluids tested (water, simulated gastric fluid, simulated intestinal fluid [fed or fasted]). Despite this, the bioavailability in preclinical species was good, which may be explained by the very high permeability of the compound. Furthermore, **17i** exhibited excellent stability both as a powder and in solution under all conditions tested, displaying no evidence for lability of the α -fluorine on the pyridine ring. The pharmacokinetics and oral bioavailability of **17i** were investigated in rat, dog, and monkey following single intravenous (as an infusion over 1 h in saline containing 2% (v/v) *N*-methylpyrrolidone and 10% (w/v) encapsin) and oral (suspended in 1% (w/v) methylcellulose in water) administration. As detailed in Table 5, good bioavailability and low blood clearance were seen across all species.

In addition to the favorable DMPK (or developability) properties outlined above and in Tables 3, 4, and 5, no time-dependent inhibition toward CYP3A4 and no formation of glutathione conjugates was observed for **17i**. This, together with weak rat and human PXR activation, gave an overall low potential for drug–drug interactions through inhibition or induction of CYP450. Additionally, the in vitro plasma protein binding of **17i** was determined in five species by equilibrium dialysis at a plasma concentration of 1 μg/mL. Table 6 demonstrates that plasma protein binding was moderate and similar across all species.

The metabolism of **17i** was investigated in vitro in liver microsomes from rat, dog, monkey, and human. Five metabolites were characterized at low abundance relative to unchanged **17i**, with four being the result of aliphatic hydroxylation.

Table 4. Preclinical Species DMPK Profiling of Pyridyl Indane Analogues^a

	17i	17j	18e
blood clearance (mL/min/kg)	5.4	55	24
$T_{1/2}$ (h)	5.0	0.6	1.0
V _{ss} (L/kg)	2.4	2.4	2.2
oral C_{max} (ng/mL)	416	116	436
oral T_{max} (h)	3	1	0.5
F (%)	61	25	72
brain–blood AUC _{0–t} ratio	2.1	1.3	1.4
microsomal CLI (mL/min/g liver) m/r/d/ma/mo/h	0.5/0.7/<0.6/0.6/1.1/<0.7	0.6/3.5/0.7/1.1/2.3/<0.6	<0.5/1.6/<0.5/0.5/1.5/<0.5
r/h PPB (%)	86.7/90.8	92.2/-	90.3/-
r BTB (%)	97.4	96.7	97.9
PAPP(+inh) (nm/s) ^b	688	633	557
P-gp efflux ratio	1.1	0.9	1.1

^a PK and CNS penetration data generated in rat, from 1 mg/kg IV or 3 mg/kg po serial and composite profiles. Species abbreviations used: m, r, d, ma, mo, h, refer to mouse, rat, dog, marmoset, monkey, and human, respectively. Plasma protein binding (PPB) and brain tissue binding (BTB) values were determined using a 96-well plate equilibrium dialysis method at a concentration of 1 μ g/mL. ^b Permeability assay defined for Table 2.

Table 5. Pharmacokinetic Parameters for 17i Obtained in Male Rat, Dog and Monkey Following Intravenous and Oral Administration^a

parameter	Sprague–Dawley rat	beagle dog	cynomolgus monkey
doses	IV 1 mg/kg po 3 mg/kg	IV 0.125 mg/kg po 0.5 mg/kg	IV 0.125 mg/kg po 0.5 mg/kg
blood clearance (mL/min/kg)	5.4 [4.6–6.3]	3.4 [3.0–4.0]	1.4 [1.3–1.5]
% liver blood flow ^b (%)	6	11	3
V _{ss} (L/kg)	2.4 [1.8–2.7]	4.8 [4.1–6.1]	1.8 [1.7–1.9]
IV half-life ($t_{1/2}$) (h)	5.0 [4.5–5.5]	16 [13–20]	15 [14–16]
oral bioavailability (%)	61 [49–70]	61 [52–70]	51 [51–52]
oral C_{max} (ng/mL)	416 [328–496]	116 [85–132]	115 [101–132]
oral T_{max} (h)	3 [2–8]	2.0 [1.3–3.0]	6 [5–8]
oral half-life ($t_{1/2}$) (h)	6.6 [6.3–7.0]	17 [15–21]	24 [22–25]

^a All parameters were calculated from blood concentration–time data. All data are reported as mean [and range], for T_{max} the median [and range] are given for $n = 3$ measurements. ^b Calculated using the following liver blood flows (mL/min/kg): rat 85, dog 31, cynomolgus monkey 44.

Table 6. In Vitro Plasma Protein Binding of 17i in Preclinical Species and Human at a Plasma Concentration of 1 μ g/mL^a

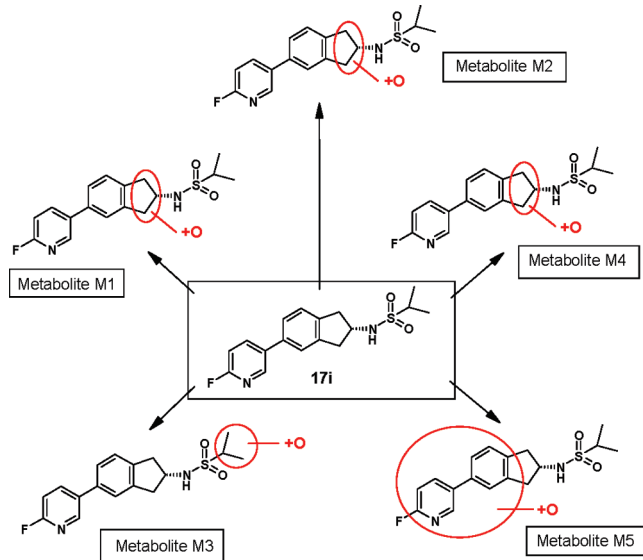
mouse	rat	dog	monkey	human
85.0 \pm 1.1	86.7 \pm 1.4	79.5 \pm 1.0	84.8 \pm 0.7	90.8 \pm 0.5

^a Results expressed as mean \pm SD of 12 determinations.

Metabolites M1, M2, and M4 (see Figure 3) were produced by oxidation of the aliphatic part of the indane ring system and probably by hydroxylation of one or both of the benzylic carbons which would result in the formation of diastereoisomers. It was not possible to determine whether M1, M2, and M4 were hydroxylated on the three carbons available or whether two were diastereoisomeric (other diastereoisomers may have been present but chromatographically unresolved from M1, M2, or M4).

In terms of relative metabolite peak areas, formation of M1 was an important metabolic route for each species. Formation of M4 was also important for rat and dog but minor in human and monkey. Formation of M2 and M3 was a relatively minor route for each species. Aryl hydroxylation (M5) was a major metabolic route in the rat but was not significant in dog, monkey, or human. All the metabolites present in human liver microsomes were also observed in rat, dog, and monkey microsomes.

Development candidate 17i exhibited no evidence of genotoxic potential in the in vitro predevelopment genetic toxicity screens. There were no significant cardiovascular risks identified from a study in cynomolgus monkeys with single oral doses up to 2.5 mg/kg, or in a hERG assay for potential effects on QT interval. Furthermore, evaluation in preclinical safety screening up to 6 weeks in duration established no observed adverse effect levels (NOAEL) with acceptable safety margins to progress into clinical evaluation.

**Figure 3.** Summary of major metabolic pathways of 17i in liver microsomes from rat, dog, human, and monkey.

The first time in human study conducted in healthy volunteers explored the pharmacokinetics of single doses of 17i in the 0.25–6 mg dose range ($N = 64$) and of a multiple dose of 0.1 mg ($N = 15$) administered daily for 28 d. According to both single and repeat dose administrations, 17i appeared to be rapidly absorbed, with C_{max} being attained between 0.5 and 3 h postdose. The apparent half-life was high on average (107–168 h) with estimated individual values up to \sim 300 h (average $t_{1/2}$ was consistent in the 0.1–6 mg dose range).

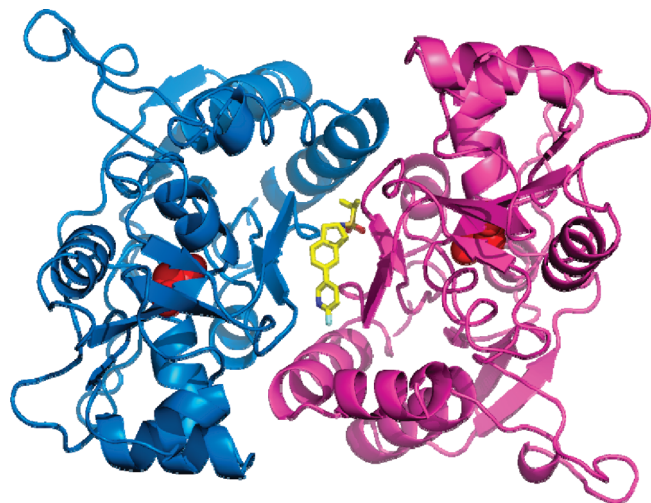


Figure 4. Crystal structure of **17i** in complex with hGluA2 S1S2 ligand binding domain. The compound (yellow carbons) binds at the dimer interface; a glutamate (red, solid) is bound at the core of each ligand binding domain.

Observed apparent oral clearance was very small, with an apparent volume of distribution in excess of total body water. A dose proportional increase in both C_{max} and AUC(0–inf) was observed following escalating single doses from 0.25 to 1.75 mg (higher doses were administered to parallel rather than interlocking cohorts). The accumulation ratio derived from the subjects receiving daily doses of **17i** for 28 d was 5.6-fold, thus confirming the PK linearity assumption. The administration of both single and multiple doses of **17i** was well tolerated: neither safety issues were raised nor withdrawals due to adverse events occurred.

Crystal Structure Determination of **17i in Complex with hGluA2 S1S2 Ligand Binding Domain.** To determine the binding mode of **17i**, we solved the crystal structure of the hGluA2 S1S2 ligand binding domain in complex with **17i** at 1.8 Å resolution. The structure showed the compound bound to the 2-fold axis of the dimer (Figure 4) in a similar manner to other AMPAR positive modulators.^{18,19,30} The compound binds in a similar manner to that described for **6**,¹⁹ with the isopropylsulphonamide group of **17i** occupying a deep pocket at the dimer interface (Supporting Information Figure).

Conclusions

In summary, a series of amino indane sulfonamide derivatives was rapidly optimized toward a series of AMPAR positive modulators with excellent drug-like physicochemical properties and good developability characteristics. This study delivered a number of molecules with encouraging rat pharmacokinetic properties, and in particular **17i**, **17j**, and **18e**, which were extensively profiled. The best overall profile was identified in **17i**, and although we were initially concerned about the lability of the *ortho*-fluoro pyridine, this group proved to be extremely stable and show no sign of chemical degradation, bioactivation risk, or metabolic susceptibility. **17i** has been proven to be safe and well tolerated in initial phase I healthy volunteer investigation and has shown the surprisingly long half-life, in excess of that predicted from preclinical species.

Experimental Section

Chemistry. General Remarks. Starting materials were obtained from commercial suppliers and used without further purifi-

cation unless otherwise stated. All reactions were conducted at ambient temperature unless otherwise stated. Flash chromatography was carried out using prepacked Isolute Flash or Biotage silica-gel columns as the stationary phase and analytical grade solvents as the eluent. Catch and release purification was carried out using SCX (strong cation exchanger) cartridges, consisting of bonded-phase silica with sulfonic acid functional groups. Mass directed preparative HPLC was carried out using a 19 mm × 100 mm or 30 mm × 100 mm, 5 μm, reversed-phase Waters Atlantis column as the stationary phase and a gradient from water +0.1% formic acid to acetonitrile +0.1% formic acid as the eluent. The eluent was monitored by a Waters 996 photodiode array and a Micromass ZQ mass spectrometer. All yields reported are of purified, isolated material. NMR spectra were obtained at 298K at the frequency stated using either a Bruker DPX400 or an Oxford Instruments 250 MHz machine and run as a dilute solution of CDCl₃ unless otherwise stated. All NMR spectra were reference to tetramethylsilane (TMS δ_H 0, δ_C 0). All coupling constants are reported in hertz (Hz), and multiplicities are labeled s (singlet), bs, (broad singlet), d (doublet), t (triplet), q (quartet), dd (doublet of doublets), dt (doublet of triplets) and m (multiplet).

Purity was determined by liquid chromatography/mass spectrometry (LC/MS) using an Agilent 1100 HPLC system with a 4.6 mm × 50 mm, 3 μm, reversed phase Waters Atlantis column as the stationary phase. A gradient elution from 97% water +0.05% formic acid/3% acetonitrile +0.05% formic acid to 97% acetonitrile +0.05% formic acid over 3 min plus a further minute continuing this mixture at a flow rate of 1.5 mL/min was used as the eluent. Retention time is reported as min (with percentage intensity for DA/ELSD for the relevant peak). Spectroscopic monitoring was performed using an Agilent 1100 diode array (DA) detector or a Sedex evaporative light scattering detector (ELSD). Total ion current traces were obtained for electrospray positive and negative ionization (ES+/ES−) and atmospheric pressure chemical positive and negative ionization (AP+/AP−). All final products were of > 95% purity by HPLC unless otherwise stated. For all key molecules, high resolution mass spectrometry data were acquired as accurate mass centroided data using a Micromass Q-ToF 2 hybrid quadrupole time-of-flight mass spectrometer, equipped with a Z-spray interface.

***N*-(2,3-Dihydro-1*H*-inden-2-yl)-2-propanesulfonamide (9).** 2-Aminoindan hydrochloride (5.16 g, 30 mmol) was suspended in dry dichloromethane (100 mL) and cooled with stirring under argon to 0 °C. To the suspension was added 1,8-diazabicyclo[5.4.0]undec-7-ene (14 g, 92 mmol) followed by the dropwise addition of isopropylsulfonyl chloride (8.56 g, 60 mmol). The cooling bath was removed and the mixture stirred at room temperature for 1 h. The reaction mixture was diluted with dichloromethane (50 mL) and washed with 1 M hydrochloric acid (2 × 50 mL). The organic layer was separated, dried over sodium sulfate, and evaporated under reduced pressure to give a yellow oil (11.8 g). The crude product was purified by chromatography on a 50 g Isolute Flash silica-gel column eluting from 20 to 50% ethyl acetate in 40–60 °C petroleum ether to give the title compound as a pale-yellow solid (6.88 g, 96%). ¹H NMR (400 MHz, CDCl₃) δ 1.39 (6H, d, *J* = 7 Hz), 2.91 (2H, m), 3.18 (1H, m), 3.31 (2H, m), 4.31 (2H, m), 7.21 (4H, m).

***N*-(5-Iodo-2,3-dihydro-1*H*-inden-2-yl)-2-propanesulfonamide (10).** *N*-(2,3-Dihydro-1*H*-inden-2-yl)-2-propanesulfonamide (1.75 g, 7.32 mmol) was dissolved in glacial acetic acid (30 mL) and then treated with concentrated sulfuric acid (0.8 mL) followed by water (2.8 mL) with stirring. This mixture was then treated with periodic acid (0.38 g, 1.67 mmol) then iodine (800 mg, 3.15 mmol), and the whole mixture was stirred at 60 °C for 4 h. The reaction mixture was allowed to cool and then partitioned between ethyl acetate (150 mL) and 10% aqueous sodium metabisulfite (100 mL). The organic layer was separated and dried over sodium sulfate and evaporated under

vacuum to give the title compound as a yellow oil (2.67 g, 100%). MS m/z 364 ($M - 1$). $^1\text{H NMR}$ (400 MHz, CDCl_3) δ 1.39 (6H, m), 3.39 (2H, m), 3.18 (1H, m), 3.28 (2H, m), 4.38 (1H, m), 4.63 (1H, m), 6.97 (1H, d, $J = 8$ Hz), 7.51 (1H, m), 7.56 (1H, m).

General Procedure for Suzuki Coupling Reactions to Prepare 11a–h. A mixture of molecule **10** (1.08 mmol) and substituted phenyl boronic acid (1.62 mmol, Combi-Blocks) in dioxane (50 mL) was treated with cesium carbonate (1.62 mmol) and water (15 mL) and degassed with argon for 2 min. Palladium(II) acetate (0.05 mmol) and triphenylphosphine (0.22 mmol) were added, and the mixture was stirred at 80 °C under argon for 16 h. The reaction mixture was cooled and then partitioned between ethyl acetate (50 mL) and water (50 mL). The organic layer was separated and dried over Na_2SO_4 and evaporated in vacuo and purified using flash chromatography.

***N*-(5-[4-((Methylsulfonyl)amino)phenyl]-2,3-dihydro-1*H*-inden-2-yl)-2-propanesulfonamide (11a).** Yield 30%. MS (ES^-) m/z 407 ($M - 1$). $^1\text{H NMR}$ (400 MHz, CDCl_3) δ 1.39 (6H, d, $J = 7$ Hz), 2.97 (2H, m), 3.05 (3H, s), 3.21 (1H, m), 3.37 (2H, m), 4.34 (1H, m), 6.52 (1H, bs), 7.18 (1H, m), 7.24 (1H, m), 7.29 (1H, d, $J = 7$ Hz), 7.40 (4H, m). HRMS (ESI) m/z 431.1064 ($[\text{M} + \text{Na}]^+$ calcd for $\text{C}_{19}\text{H}_{24}\text{NaN}_2\text{O}_4\text{S}_2^+$ 431.1075).

***N*-(5-(3-Cyanophenyl)-2,3-dihydro-1*H*-inden-2-yl)-2-propanesulfonamide (11c).** Yield 73%. MS (ES^-) m/z 339 ($M - 1$). $^1\text{H NMR}$ (400 MHz, CDCl_3): 1.41 (6H, d, $J = 7$ Hz), 2.98 (2H, m), 3.21 (1H, m), 3.38 (2H, m), 4.37 (2H, m), 7.32 (1H, d, $J = 8$ Hz), 7.39 (2H, m), 7.53 (1H, m), 7.62 (1H, m), 7.78 (1H, m), 7.83 (1H, m).

***N*-(5-[3-(Methyl(methylsulfonyl)amino)phenyl]-2,3-dihydro-1*H*-inden-2-yl)-2-propanesulfonamide (11h).** Yield 63%. MS (ES^-) m/z 359 ($M - 1$). $^1\text{H NMR}$ (400 MHz, CDCl_3) δ 1.38 (6H, m), 2.99 (2H, m), 3.18 (1H, m), 3.38 (2H, m), 4.35 (2H, m), 7.34 (1H, d $J = 8$ Hz), 7.45 (2H, m), 7.60 (1H, m), 7.88 (1H, dd, $J = 8$ and 1 Hz), 8.19 (1H, m), 8.41 (1H, m).

***N*-(5-[3-(Aminomethyl)phenyl]-2,3-dihydro-1*H*-inden-2-yl)-2-propanesulfonamide (14).** A 1.0 M solution of lithium aluminum hydride in tetrahydrofuran (8 mL) was cooled to 0 °C in an ice/methanol bath with stirring under argon. The solution was then treated dropwise with a solution of *N*-(5-(3-cyanophenyl)-2,3-dihydro-1*H*-inden-2-yl)-2-propanesulfonamide (**11c**) (0.67 g, 1.97 mmol) in dry tetrahydrofuran (20 mL) over 15 min. The cooling bath was removed and the whole mixture stirred at reflux for 2 h. The reaction mixture was allowed to cool to room temperature and quenched with water (0.8 mL), 10% NaOH (0.8 mL), and water again (1.2 mL). The reaction mix was dried over sodium sulfate, filtered, and the filtrate evaporated under reduced pressure to give the **14** as a yellow oil (0.67 g, 100%). MS (ES^+) m/z 345 ($M + 1$). $^1\text{H NMR}$ (400 MHz, CDCl_3): 1.40 (6H, d, $J = 7$ Hz), 1.66 (2H, m), 2.96 (2H, m), 3.19 (1H, m), 3.36 (2H, m), 3.91 (2H, m), 4.33 (1H, m), 4.67 (1H, m), 7.27 (2H, m), 7.40 (4H, m), 7.49 (1H, s).

***N*-(5-[3-[(2-Oxo-1-pyrrolidinyl)methyl]phenyl]-2,3-dihydro-1*H*-inden-2-yl)-2-propanesulfonamide (15).** A solution of *N*-(5-[3-(aminomethyl)phenyl]-2,3-dihydro-1*H*-inden-2-yl)-2-propanesulfonamide (**14**) (69 mg, 0.2 mmol) in dichloromethane (5 mL) was treated with triethylamine (40 mg, 0.4 mmol), followed by 4-chlorobutanoyl chloride (32 mg, 0.22 mmol), and the whole mixture stirred at room temperature under argon for 1 h. The reaction mixture was evaporated under reduced pressure to remove the dichloromethane and then dimethylformamide was added (5 mL) followed by potassium carbonate (60 mg, 0.43 mmol) and the mixture stirred at 100 °C for 2 h. The reaction mixture was cooled and then partitioned between dichloromethane and 0.5 M hydrochloric acid, and the organic layer was evaporated under reduced pressure to give a brown oil which was purified by column chromatography on a 1 g SCX column eluting from 0 to 50% ethyl acetate in 40–60 °C petroleum ether to give **15** as a beige solid (16 mg, 19%). MS (ES^+) m/z 413 ($M + 1$). $^1\text{H NMR}$ (400 MHz, CDCl_3): 1.41 (6H, d, $J = 7$ Hz), 2.00 (2H, m), 2.45 (2H, m), 2.96 (2H, m), 3.21 (1H,

m), 3.30 (2H, m), 3.38 (2H, m), 4.35 (2H, m), 4.51 (2H, s), 7.22 (1H, m), 7.28 (1H, d, $J = 8$ Hz), 7.40 (4H, m), 7.47 (1H, m). HRMS (ES^+) m/z 413.1883 ($[\text{M} + \text{H}]^+$ calcd for $\text{C}_{23}\text{H}_{29}\text{N}_2\text{O}_3\text{S}^+$ 413.1899).

(*S*)-5-Bromo-2-aminoindan (Camphorsulfonate Salt) (20). Compound **20** was prepared using a similar method to that described in the literature,²⁷ i.e., by resolution of the free base form of racemic 5-bromo-2-aminoindane using (1*R*)-(–)-10-camphorsulphonic acid to obtain (*S*)-5-bromo-2-aminoindan (1*R*)-(–)-10-camphorsulfonate salt. The absolute configuration of (*S*)-5-bromo-2-aminoindan (1*R*)-(–)-10-camphorsulfonate salt was confirmed by X-ray crystallography. Furthermore, the enantiomeric purity of (*S*)-5-bromo-2-aminoindan (1*R*)-(–)-10-camphorsulfonate salt was checked by HPLC using the following conditions: Column, chiralpak AD-H 5 μm , 250 mm \times 4.6 mm. Mobile phase: A, *n*-hexane; B, ethanol + 0.1% isopropyl amine (gradient: isocratic 8% B, flow rate: 0.8 mL/min; UV WL range: 200–400 nm; analysis time: 17 min). Enantiomer 1 was recovered as 0.84% a/a from the racemate (retention time = 11.9 min). Enantiomer 2 was recovered as 99.16% a/a from the racemate (retention time = 12.8 min).

***N*-(2*S*)-5-Bromo-2,3-dihydro-1*H*-inden-2-yl)-2-propanesulfonamide (21).** Compound **20** was treated with NaOH (1 M solution in water to reach pH = 10) in isopropyl acetate as solvent. The free base form of **20** was converted to **21** as for racemic mixture **9**.

***N*-(2*S*)-5-(6-Fluoro-3-pyridinyl)-2,3-dihydro-1*H*-inden-2-yl)-2-propanesulfonamide (17i).** Compound **21** was reacted with (6-fluoro-3-pyridinyl)boronic acid in a similar process used for the preparation of **17c**. The enantiomeric purity of **17i** was checked by HPLC using the following conditions: column, Chiralpak AS-H 5 μm , 250 mm \times 4.6 mm. Mobile phase: A, *n*-hexane; B, ethanol. Gradient, isocratic 30% B; flow rate, 0.8 mL/min; UV WL range, 200–400 nm; analysis time, 20 min. Enantiomer 1 was recovered as 2.08% a/a from the racemate (retention time = 16.3 min). Enantiomer 2 was recovered as 97.92% a/a from the racemate (retention time = 17.7 min). Enantiomer 2 was confirmed to be *N*-[(2*S*)-5-(6-fluoro-3-pyridinyl)-2,3-dihydro-1*H*-inden-2-yl]-2-propanesulfonamide by X-ray crystallography. Relevant IR bands: 3154 cm^{-1} Str. NH, 1600 cm^{-1} Str. C=N, C=C, 1314 cm^{-1} Str. SO₂, 1141–1125 cm^{-1} Str. SO₂, Str. C–F. $^1\text{H NMR}$ as **17c**. $^{13}\text{C NMR}$ (150 MHz, $\text{DMSO}-d_6$): δ 162.3, 145.1, 141.8, 140.9, 134.5, 134.4, 125.3, 125.0, 122.8, 109.5, 54.1, 51.7, 39.9, 40.0, 16.4. HRMS (ES^+) m/z 335.1220 ($[\text{M} + \text{H}]^+$ calcd for $\text{C}_{17}\text{H}_{20}\text{N}_2\text{O}_2\text{FS}^+$ 335.1230).

***N*-(2*R*)-5-(6-Fluoro-3-pyridinyl)-2,3-dihydro-1*H*-inden-2-yl)-2-propanesulfonamide (17h).** compound **17h** was prepared by an analogous sequence using (*S*)-camphor sulfonic acid as resolving agent. The enantiomeric purity of **17h** obtained was checked by HPLC using the same conditions as for the **17i**. Enantiomer 1 was recovered as 99.04% a/a from the racemate (retention time = 16.62 min). Enantiomer 2 was recovered as 0.96% a/a from the racemate (retention time = 18.29 min). HRMS (ES^+) m/z 335.1230 ($[\text{M} + \text{H}]^+$ calcd for $\text{C}_{17}\text{H}_{20}\text{N}_2\text{O}_2\text{FS}^+$ 335.1230).

***N*-(2*S*)-5-(6-Methyl-3-pyridinyl)-2,3-dihydro-1*H*-inden-2-yl)-2-propanesulfonamide (17j).** A mixture of *N*-[(2*S*)-5-(4,4,5,5-tetramethyl-1,3,2-dioxaborolan-2-yl)-2,3-dihydro-1*H*-inden-2-yl]-2-propanesulfonamide **24** (1.27 g, 3.48 mmol), 2-methyl-5-bromopyridine (1.1 eq, 658 mg, 3.82 mmol), and cesium carbonate (1.7 g, 5.22 mmol) in a 3:1 mixture of 1,4-dioxane: water (13 mL) was degassed with argon for 5 min. Polymer bound tetrakis(triphenylphosphine)-palladium (5% mol, 1.74 g, 0.17 mmol) was then added, and the whole mixture stirred at 125 °C for 30 min in a microwave reactor. The reaction mixture was allowed to cool and filtered over a celite pad. The filtrate was partitioned between ethyl acetate (50 mL) and water (50 mL). Phases were separated, and the aqueous was back extracted with ethyl acetate (2 \times 50 mL). Combined organic layers were washed

with brine (2 × 50 mL), dried, and evaporated under reduced pressure to give an orange oil, which was purified by Flash silica-gel column, eluting from 40 to 45% ethyl acetate in cyclohexane to give the title compound as a white solid (655 mg, 57%). MS (ES+) m/z 331 (M + 1). ¹H NMR (400 MHz, CDCl₃): 1.41 (6H, m), 2.60 (3H, s), 2.97 (2H, m), 3.20 (1H, m), 3.38 (2H, m), 4.35 (2H, m), 7.21 (1H, d, J = 8 Hz), 7.30 (1H, m), 7.38 (2H, m), 7.73 (1H, dd, J = 8 Hz and 2 Hz), 8.68 (1H, d, J = 2 Hz). HRMS (ES+) m/z 331.1471 ([M + H]⁺ calcd for C₁₈H₂₃N₂O₂S⁺ 331.1480).

***N*-[(2*S*)-5-(5-Fluoro-2-pyridinyl)-2,3-dihydro-1*H*-inden-2-yl]-2-propanesulfonamide (18e).** A mixture of *N*-[(2*S*)-5-(4,4,5,5-tetramethyl-1,3,2-dioxaborolan-2-yl)-2,3-dihydro-1*H*-inden-2-yl]-2-propanesulfonamide **24** (48.5 g, 0.133 mol), 2-bromo-5-fluoropyridine (26.9 g, 0.15 mol), and cesium carbonate (1 M water solution, 270 mL, 0.266 mol) in 1,4-dioxane (490 mL) was degassed with argon for 5 min. Polymer bound tetrakis(triphenylphosphine)-palladium (1% mol, 2.66 g, 1.33 mmol) was then added and the whole mixture stirred at 83 °C for 3 h. The reaction mixture was allowed to cool and filtered over a celite pad. The filtrate was partitioned between ethyl acetate (500 mL) and water (500 mL). Phases were separated, and the aqueous was back-extracted with ethyl acetate (2 × 500 mL). Combined organic layers were washed with brine (2 × 500 mL), dried, and evaporated under reduced pressure to give an orange oil, which was purified by Flash silica-gel column, eluting from 10 to 20% ethyl acetate in cyclohexane to give the title compound as a white solid (35 g, 79%). MS (APCI) m/z 335 (M + 1). ¹H NMR (400 MHz, CDCl₃): 1.40 (6H, m), 2.96 (2H, m), 3.20 (1H, m), 3.38 (2H, m), 4.34 (2H, m), 7.31 (1H, m), 7.47 (1H, m), 7.71 (2H, m), 7.81 (1H, m), 8.52 (1H, m). HRMS (ES+) m/z 335.1217 ([M + H]⁺ calcd for C₁₇H₂₀N₂O₂FS⁺ 335.1230).

Calcium Influx Fluorescence Assay. Stable HEK293-hGluR2-iQ/R unedited cells were grown in a DMEM/F12, 10% FBS in a 5% CO₂ incubator in 175 cm² T-flasks. Two–three d before experiment, cells were detached and seeded into 384-well black PDL-coated plates with clear bottom up to confluence. On the day of the experiment, cell plates were washed 3 times with assay buffer (in mM): 20 HEPES, 145 NaCl, 5 KCl, 2 CaCl₂, 1 MgCl₂, 5.5 glucose, pH 7.3, and loaded with 2 μM Fluo4 AM for 60 min at room temperature. Cell plates were washed again to remove unloaded Fluo4 and placed into a FLIPR. A dual addition protocol was used to add compound solution 5 min before 100 μM glutamate stimulation. The glutamate-induced increased fluorescence was analyzed by using ActivityBase software and compared with positive control cyclothiazide.

Whole Cell Voltage-Clamp Electrophysiology Assay. This assay involved the electrophysiological characterization of AMPA receptor positive modulators using HEK293 cells stably expressing human GluA2 flip (unedited) subunits which form a functional homotetrameric AMPA receptor. The extracellular recording solution contained (in mM): 140 NaCl, 2 KCl, 1 MgCl₂, 2 CaCl₂, 12 *N*-[2-hydroxyethyl]-piperazine-*N*-[2-ethanesulfonic acid (HEPES), 10 D-glucose, pH 7.35. The intracellular solution contained (in mM): 150 CsCl, 10 HEPES, 10 ethylene glycol-bis-(γ -aminoethylether)-*N,N,N',N'*-tetra-acetic acid (EGTA), pH 7.3. For perforated patch recordings intracellular solution containing amphotericin B (240 μg/mL) was used to backfill the pipet while intracellular solution alone was used to fill just the tip (the patch clamp pipettes have a resistance of between 2 and 5 MΩ). Amphotericin B creates small pores in the cell membrane beneath the electrode which allow small ions to pass across the membrane (and therefore allow electrical control of the cell) without the dialysis of second messenger molecules out of the cell, which could result in metabolic rundown of the cell leading to inconsistent receptor activation.³¹ The membrane potential of the cell was held at -60 mV and perforated patch clamp electrophysiology performed using EPC9 or 10 patch clamp system. The cell was positioned in front of the first of 16 linearly arranged channels. The system moves one channel and then the next in

front of a single patch-clamped cell, allowing rapid exchange and precise application times of solutions (for more information see <http://www.cellectricon.se/>). The first channel contained normal buffer for baseline current measurement. The second channel contained 3 mM glutamate, which was applied to the cell for 500 ms to record a control (agonist alone) response. The third channel contained normal buffer, which washed off glutamate for 1–3 min. The fourth channel, which contained either a compound of the invention or a reference compound, was moved in front of the cell for one minute. The fifth channel contained glutamate in the presence of the test (or reference) compound, which was applied to the cell for 500 ms. The sixth channel contained normal buffer, which washed off the glutamate plus test (or reference) compound for 1–3 min. This procedure was repeated for increasing concentrations of either a compound of the invention or a reference compound. The activity of a compound of the invention is determined by measuring the peak current amplitude or the area under the curve (500 ms) for the glutamate response in the presence of the compound of the invention (or reference) and expressing it as % of potentiation of the response to glutamate alone.

P450 CYP_{EX} Assay. Inhibition (IC₅₀) of human CYP1A2, 2C9, 2C19, 2D6, and 3A4 was determined using Cypex Bactosomes expressing the major human P450s. A range of concentrations (0.1, 0.2, 0.4, 1, 2, 4, and 10 μM) of test compound were prepared in methanol and preincubated at 37 °C for 10 min in 50 mM potassium phosphate buffer (pH 7.4) containing recombinant human CYP450 microsomal protein (0.1 mg/mL; Cypex Limited, Dundee, UK) and probe-fluorescent substrate. The final concentration of solvent was between 3 and 4.5% of the final volume. Following preincubation, NADPH regenerating system (7.8 mg glucose 6-phosphate, 1.7 mg NADP, and 6 units glucose-6-phosphate dehydrogenase/mL of 2% (w/v) NaHCO₃; 25 μL) was added to each well to start the reaction. Production of fluorescent metabolite was then measured over a 10 min time course using a Spectrafluor plus plate reader. The rate of metabolite production (AFU/min) was determined at each concentration of compound and converted to a percentage of the mean control rate using Magellan (Tecan software). The inhibition (IC₅₀) of each compound was determined from the slope of the plot using Grafit v5 (Erithacus software, UK). Miconazole was added as a positive control to each plate. CYP450 isoform substrates used were ethoxyresorufin (ER; 1A2; 0.5 μM), 7-methoxy-4-trifluoromethylcoumarin-3-acetic acid (FCA; 2C9; 50 μM), 3-butyryl-7-methoxycoumarin (BMC; 2C19; 10 μM), 4-methylaminomethyl-7-methoxycoumarin (MMC; 2D6; 10 μM), diethoxyfluorescein (DEF; 3A4; 1 μM), and 7-benzyloxyquinoline (7-BQ; 3A4; 25 μM). The test was performed in three replicates.

Intrinsic Clearance (CL_i) Assay. Intrinsic clearance (CL_i) values were determined in rat and human liver microsomes. Test compounds (0.5 μM) were incubated at 37 °C for 30 min in 50 mM potassium phosphate buffer (pH 7.4) containing 0.5 mg microsomal protein/mL. The reaction was started by addition of cofactor (NADPH; 8 mg/mL). The final concentration of solvent was 1% of the final volume. At 0, 3, 6, 9, 15, and 30 min, an aliquot (50 μL) was taken, quenched with acetonitrile containing an appropriate internal standard, and analyzed by HPLC-MS/MS. The intrinsic clearance (CL_i) was determined from the first-order elimination constant by nonlinear regression using Grafit v5 (Erithacus software, UK), corrected for the volume of the incubation and assuming 52.5 mg microsomal protein/g liver for all species. Values for CL_i were expressed as mL/min/g liver. The lower limit of quantification of clearance was determined to be when <15% of the compound had been metabolized by 30 min, and this corresponded to a CL_i value of 0.5 mL/min/g liver. The upper limit was 50 mL/min/g liver.

Determination of the X-ray Structure of Human AMPA Human Glutamate Receptor GluA2 S1S2 Ligand Binding Domain with 17i. Construct Generation, Expression, and Purification. To construct the pET15b-humanGluA2flipS1-GlyThr-S2 plasmid

the DNA fragments, S1 and S2 were amplified in separate polymerase chain reactions. The pCDNA3.2-humanGluA2flip plasmid was used as a template for amplification of the hGluA2-flip S1 and S2 fragments. The primers for the S1 reaction were, 5'hGluA2flipS1: 5'-CGATCCATATGGGCTCTGGAAATG-ACACCTCTGGG-3' and 3'hGluA2flipS1: 5'-TTCGATGGG-GGTGCCCTTCTTGATCATGATAGATATC-3'; the primers for amplification of S2 were 5'hGluA2flipS2: 5'-ATCAA GAAGGGACCCCCATCGAAAGTGCTGAGGATC-3' and 3'hGluA2flipS2: 5'-GGATCCTCGAGGGCTCCACATTCACCTTATC-3'; the underlined sequences are complementary to the template. Each 100 mL of PCR used 100 ng of pCDNA-3.1-humanGluA2flip template, 25 pmol of each primer, 40 mM of each dNTP, 5U of Pfu DNA polymerase, and 25 cycles of amplification. The major products were of the predicted size and were gel purified and eluted into 30 mL of water. Two ml of each product and primers 5'hGluA2flipS1 and 3'hGluA2flipS2 were used in a second round of PCR using the complementary overlapping regions to amplify the full length S1-GlyThr-S2 fragment. The S1-GlyThr-S2 fragment and the vector, pET15b, were digested with NdeI and XhoI. Subsequently, all digest products were gel purified; S1-GlyThr-S2 was ligated into the pET15b vector to generate pET15b-humanGluA2flipS1-GlyThr-S2. This was verified by sequencing.

Expression and Purification of S1S2 Ligand Binding Domain. pET15b-humanGluA2flipS1-GlyThr-S2 was transformed into *Escherichia coli* BL21(DE3) for expression. Overnight cultures grown in LB containing 100 µg/mL carbenicillin were diluted into fresh media, grown at 37 °C to an OD₆₀₀ of ~0.8 and induced with 1 mM IPTG. After 4 h induction, cells were harvested by centrifugation and inclusion bodies prepared. Cell paste, resuspended to 25% (w/v) in Tris buffer (50 mM Tris, pH 8.0, 0.2 M NaCl, 1 mM EDTA), was incubated with 20 µg/mL lysozyme and the cells broken on a Manton Gaulin homogenizer. After addition of Triton X-100 to 2% (w/v), the pellet was harvested by centrifugation and washed twice by resuspending in Tris buffer containing 1 M NaCl and 5 mM DTT, each time recovering the pellet by centrifugation. The final pellet was resuspended in a minimum volume of Tris buffer plus 5 mM DTT. Then 500 mg aliquots of resuspended inclusion body were solubilized in guanidine and refolded and purified exactly according to the method of Chen et al.³²

LC/MS analysis confirmed purification of protein with the expected mass of 29237 Da. Purified protein was dialyzed exhaustively against 10 mM Hepes pH 7.0, 20 mM NaCl, 1 mM EDTA, concentrated to 18–20 mg/mL, flash frozen in liquid nitrogen, and stored at –80 °C.

Crystallization. Protein was incubated with solid compound at 4 °C overnight. The sample was then spun at 4 °C/13.2 rpm/15 min in a microfuge and screened with a grid of (18, 20, 22, 24%) peg 8K, 0.1 M sodium acetate at pH 5.0, 0.2 M ammonium sulfate) in a 24-well VDX plate using the hanging drop method (1 + 1 µL drops). Crystal quality was improved by hair-seeding. Crystals were harvested by transferring into well solution plus 15% glycerol for approximately 10 s, followed by flash freezing in liquid nitrogen.

Data Collection and Structure Solution. X-ray diffraction data were collected at the ESRF on BL23. Data were processed with DENZO and scaled with SCALEPACK,³³ resulting in an R_{merge} of 7.3%. The structure was solved by molecular replacement using the rat GluA2 S1S2J-N754S with CTZ (PDB code 1LBC) using AMORE.³⁴ Prior to molecular replacement, the cyclothiazide and water molecules were removed and the residues that differed between the rat and human protein were changed to alanine. Model building was carried out using the program O,³⁵ and refinement was carried out with CNX using standard positional refinement and B -factor refinement protocols.³⁶ The final R_{work} was 19.8% and R_{free} was 23.6% for data between the resolution of 20 and 1.8 Å. The final model contains 569 water molecules, 2 glutamate molecules, 5 sulfate molecules, and 2 **17i** molecules (final statistics in Supporting Information Table 1). The four re-

sidues (Arg231, Thr232, Pro233, Val246) that differ in sequence between the rat and human S1S2 ligand binding domain are not close to the positive modulator binding site and do not affect binding of **17i**. The atomic coordinates for the crystal structure described here have been deposited at the Protein Data Bank under entry code 2xhd.

Acknowledgment. We thank Dr. Bill Leavens for generating the HRMS data.

Supporting Information Available: Full experimental procedures and characterization for all compounds not included above. Plasma protein binding of **17i** in mouse, rat, dog, cynomolgus monkey, and human and brain tissue binding in the rat. Methods for membrane permeability, P-glycoprotein transport, and interaction and analysis of blood, plasma, or brain samples from in vivo and protein binding studies. High resolution mass spectrometry methods and comparison of the crystal structure of **6** and **17i**. This material is available free of charge via the Internet at <http://pubs.acs.org>.

References

- (1) Sanacora, G.; Zarate, C. A.; Krystal, J. H.; Manji, H. K. Targeting the glutamatergic system to develop novel, improved therapeutics for mood disorders. *Nature Rev. Drug Discovery* **2008**, *7*, 426–437.
- (2) Zarate, C. A., Jr.; Manji, H. K. The role of AMPA receptor modulation in the treatment of neuropsychiatric diseases. *Exp. Neurol.* **2008**, *211*, 7–10.
- (3) Black, M. D. Therapeutic potential of positive AMPA modulators and their relationship to AMPA receptor subunits. A review of preclinical data. *Psychopharmacology (Berlin)* **2005**, *179*, 154–163.
- (4) Granger, R.; Staubli, U.; Davis, M.; Perez, Y.; Nilsson, L.; Rogers, G. A.; Lynch, G. A drug that facilitates glutamatergic transmission reduces exploratory activity and improves performance in a learning-dependent task. *Synapse* **1993**, *15*, 326–329.
- (5) Lynch, G.; Gall, C. M. Ampakines and the threefold path to cognitive enhancement. *Trends Neurosci.* **2006**, *29*, 554–562.
- (6) Dingledine, R.; Borges, K.; Bowie, D.; Traynelis, S. F. The glutamate receptor ion channels. *Pharmacol. Rev.* **1999**, *51*, 7–61.
- (7) Ozawa, S.; Kamiya, H.; Tsuzuki, K. Glutamate receptors in the mammalian central nervous system. *Prog. Neurobiol.* **1998**, *54*, 581–618.
- (8) Mansour, M.; Nagarajan, N.; Nehring, R. B.; Clements, J. D.; Rosenmund, C. Heteromeric AMPA receptors assemble with a preferred subunit stoichiometry and spatial arrangement. *Neuron* **2001**, *32*, 841–853.
- (9) Tichelaar, W.; Safferling, M.; Keinanen, K.; Stark, H.; Madden, D. R. The Three-dimensional Structure of an Ionotropic Glutamate Receptor Reveals a Dimer-of-Dimers Assembly. *J. Mol. Biol.* **2004**, *344*, 435–442.
- (10) Armstrong, N.; Gouaux, E. Mechanisms for activation and antagonism of an AMPA-sensitive glutamate receptor: crystal structures of the GluR2 ligand binding core. *Neuron* **2000**, *28*, 165–181.
- (11) Gouaux, E. Structure and function of AMPA receptors. *J. Physiol.* **2004**, *554*, 249–253.
- (12) Collingridge, G. L.; Isaac, J. T.; Wang, Y. T. Receptor trafficking and synaptic plasticity. *Nature Rev. Neurosci.* **2004**, *5*, 952–962.
- (13) Milstein, A. D.; Nicoll, R. A. Regulation of AMPA receptor gating and pharmacology by TARP auxiliary subunits. *Trends Pharmacol. Sci.* **2008**, *29*, 333–339.
- (14) Tomita, S.; Adesnik, H.; Sekiguchi, M.; Zhang, W.; Wada, K.; Howe, J. R.; Nicoll, R. A.; Bredt, D. S. Stargazin modulates AMPA receptor gating and trafficking by distinct domains. *Nature* **2005**, *435*, 1052–1058.
- (15) Soto, D.; Coombs, I. D.; Kelly, L.; Farrant, M.; Cull-Candy, S. G. Stargazin attenuates intracellular polyamine block of calcium-permeable AMPA receptors. *Nature Neurosci.* **2007**, *10*, 1260–1267.
- (16) Kuusinen, A.; Arvola, M.; Keinanen, K. Molecular dissection of the agonist binding site of an AMPA receptor. *EMBO J.* **1995**, *14*, 6327–6332.
- (17) Armstrong, N.; Sun, Y.; Chen, G. Q.; Gouaux, E. Structure of a glutamate-receptor ligand-binding core in complex with kainate. *Nature* **1998**, *395*, 913–917.
- (18) Jin, R.; Clark, S.; Weeks, A. M.; Dudman, J. T.; Gouaux, E.; Partin, K. M. Mechanism of positive allosteric modulators acting on AMPA receptors. *J. Neurosci.* **2005**, *25*, 9027–9036.

- (19) Sobolevsky, A. I.; Rosconi, M. P.; Gouaux, E. X-ray structure, symmetry and mechanism of an AMPA-subtype glutamate receptor. *Nature* **2009**, *462*, 745–756.
- (20) Sommer, B.; Keinänen, K.; Verdoorn, T. A.; Wisden, W.; Burnashev, N.; Herb, A.; Kohler, M.; Takagi, T.; Sakmann, B.; Seeburg, P. H. Flip and flop: a cell-specific functional switch in glutamate-operated channels of the CNS. *Science* **1990**, *249*, 1580–1585.
- (21) Leever, J. D.; Clark, S.; Weeks, A. M.; Partin, K. M. Identification of a site in GluR1 and GluR2 that is important for modulation of deactivation and desensitization. *Mol. Pharmacol.* **2003**, *64*, 5–10.
- (22) Harpsoe, K.; Liljefors, T.; Balle, T. Prediction of the binding mode of biarylpropylsulfonamide allosteric AMPA receptor modulators based on docking, GRID molecular interaction fields and 3D-QSAR analysis. *J. Mol. Graphics Modell.* **2008**, *26*, 874–883.
- (23) Morrow, J. A.; Maclean, J. K.; Jamieson, C. Recent advances in positive allosteric modulators of the AMPA receptor. *Curr. Opin. Drug Discovery Dev.* **2006**, *9*, 571–579.
- (24) Francotte, P.; de Tullio, P.; Fraikin, P.; Counerotte, S.; Goffin, E.; Pirote, B. In search of novel AMPA potentiators. *Recent Pat. CNS Drug Discovery* **2006**, *1*, 239–246.
- (25) Ward, S. E.; Bax, B. D.; Harries, M. Challenges for and current status of research into positive modulators of AMPA receptors. *Br. J. Pharmacol.* **2010**, *160*, 181–190.
- (26) Subramanian, G.; Kitchen, D. B. Computational models to predict blood–brain barrier permeation and CNS activity. *J. Comput.-Aided Mol. Des.* **2003**, *17*, 643–664.
- (27) Prashad, M.; Hu, B.; Har, D.; Repic, O.; Blacklock, T. J.; Acemoglu, M. Efficient and practical syntheses of (*R*)-(5-amino-2,3-dihydro-1*H*-inden-2-yl)carbamic acid methyl ester. *Adv. Synth. Catal.* **2001**, *343*, 461–472.
- (28) Ennaceur, A.; Delacour, J. A new one-trial test for neurobiological studies of memory in rats. 1: Behavioral data. *Behav. Brain Res.* **1988**, *31*, 47–59.
- (29) Foley, A. G.; Murphy, K. J.; Hirst, W. D.; Gallagher, H. C.; Hagan, J. J.; Upton, N.; Walsh, F. S.; Regan, C. M. The 5-HT(6) receptor antagonist SB-271046 reverses scopolamine-disrupted consolidation of a passive avoidance task and ameliorates spatial task deficits in aged rats. *Neuropsychopharmacology* **2004**, *29*, 93–100.
- (30) Hald, H.; Ahring, P. K.; Timmermann, D. B.; Liljefors, T.; Gajhede, M.; Kastrup, J. S. Distinct structural features of cyclothiazide are responsible for effects on peak current amplitude and desensitization kinetics at iGluR2. *J. Mol. Biol.* **2009**, *391*, 906–917.
- (31) Virginio, C.; Giacometti, A.; Aldegheri, L.; Rimland, J. M.; Terstappen, G. C. Pharmacological properties of rat alpha 7 nicotinic receptors expressed in native and recombinant cell systems. *Eur. J. Pharmacol.* **2002**, *445*, 153–161.
- (32) Chen, P. E.; Wyllie, D. J. Pharmacological insights obtained from structure–function studies of ionotropic glutamate receptors. *Br. J. Pharmacol.* **2006**, *147*, 839–853.
- (33) Otwinowski, Z. Data collection and processing. In *Proceedings of CCP4 Study Weekend*; Sawyer, L., Ed.; SERC Daresbury Laboratory: Warrington, UK: 1993; pp 56–62.
- (34) Bailey, S. The CCP4 suite: programs for protein crystallography. *Acta Crystallogr., Sect. D: Biol. Crystallogr.* **1994**, *50*, 760–763.
- (35) Jones, T. A.; Zou, J. Y.; Cowan, S. W.; Kjeldgaard, M. Improved methods for building protein models in electron density maps and the location of errors in these models. *Acta Crystallogr., Sect. A: Found. Crystallogr.* **1991**, *47*, 110–119.
- (36) Brunger, A. T.; Adams, P. D.; Clore, G. M.; DeLano, W. L.; Gros, P.; Grosse-Kunstleve, R. W.; Jiang, J. S.; Kuszewski, J.; Nilges, M.; Pannu, N. S.; Read, R. J.; Rice, L. M.; Simonson, T.; Warren, G. L. Crystallography & NMR system: A new software suite for macromolecular structure determination. *Acta Crystallogr., Sect. D: Biol. Crystallogr.* **1998**, *54*, 905–921.